Suppression of MHD Fluctuations Leading to Improved Confinement in a Gun-Driven Spheromak

H. S. McLean, S. Woodruff, E. B. Hooper, R. H. Bulmer, D. N. Hill, C. Holcomb, J. Moller, B. W. Stallard, R. D. Wood, and Z. Wang*

Lawrence Livermore National Laboratory, Livermore, California 94550

(Received 12 July 2001; published 8 March 2002)

Magnetic fluctuations have been reduced to ~1% during discharges on the Sustained Spheromak Physics Experiment by shaping the spatial distribution of the bias magnetic flux in the device. In the resulting quiescent regime, the safety factor profile is nearly flat in the plasma and the dominant ideal and resistive MHD modes are greatly reduced. During this period, the temperature profile is peaked at the magnetic axis and maps onto magnetic flux contours. Energy confinement time is improved over previous reports in a driven spheromak.

DOI: 10.1103/PhysRevLett.88.125004 PACS numbers: 52.55.Hc, 52.30.Cv, 52.35.Py

In this Letter we show, for the first time, that magnetic fluctuations can be controlled in a driven spheromak, leading to a nearly quiescent regime giving the highest beta, highest electron temperature, and longest confinement time yet observed for a spheromak continuously driven by helicity injection. Magnetic fluctuations are responsible for both energy gain (current drive with associated Ohmic heating) and energy loss (heat transport) in spheromaks, and are driven by spatial gradients in the ratio of current density to magnetic field, $\lambda \equiv \mu_0 \boldsymbol{j} \cdot \boldsymbol{B}/B^2$, where $\boldsymbol{j}$ is the current density and $\boldsymbol{B}$ is the magnetic field [1]. Understanding the balancing of current drive and energy transport, both the result of fluctuations, is necessary to produce high temperature, low collisionality sustained plasmas.

In toroidal magnetically confined plasmas, such as the spheromak or reversed field pinch (RFP), energy transport is enhanced when fluctuations in the magnetic field break magnetic surfaces, allowing energy loss to the walls [2]. Typically, instabilities occur near mode-rational surfaces (i.e., where the safety factor $q = m/n$, $q \equiv d\Phi/d\psi$, $m =$ dominant poloidal mode number, $n =$ toroidal mode number, $\Phi =$ toroidal flux, $\psi =$ poloidal flux). An Ohmically driven RFP [3] exhibits a spectrum of modes due to a q profile that falls from ~0.2 in the core to <0 at the wall, typically $m = 0, 1$ and $n = 5$–10. In contrast, for a spheromak with substantial edge current, the q profile spans few resonant surfaces ($0.5 < q < 1.0$), leading to only a few $m = 1$ modes [4], typically $n \leq 4$. Fluctuation amplitudes in spheromaks, however, have generally been much larger than RFPs, resulting in poorer confinement.

Large fluctuations are seen at the extremes of high and low edge currents in spheromaks. In a magnetized coaxial gun-driven spheromak, current drive is provided by a plasma dynamo [5], through which currents flowing on external open field lines couple to internal currents flowing on closed (or nearly closed) flux surfaces. With higher external edge currents, the $n = 1$ mode is observed resulting from a kinked distortion of the current on the open flux. It is this low order mode that is understood to provide the fluctuation power that couples current from the open magnetic flux into the spheromak [6]. Higher mode number magnetic turbulence then distributes current throughout the spheromak core [7]. When the external currents are reduced, $n = 2, 3, 4$ modes are observed. The latter result from resistivity-profile effects, in which the current in a warm core decays less rapidly than current at the edge [8].

Conventional guns have a threshold in the discharge current required to form a spheromak that also produces excessive edge current and fluctuations after formation. This results from the single solenoid with magnetic field lines that diverge radially near the muzzle of the gun. To eject plasma, the gun current must rise enough to bend these field lines and expand them from the gun into the flux conserver. The threshold condition is $\lambda > \lambda_{\text{gun}}$, where $\lambda_{\text{gun}} \equiv \pi/\Delta$. (In the gun, $\lambda = \mu_0 j/B = \mu_0 I_{\text{gun}}/\Phi_{\text{gun}}$, $I_{\text{gun}} =$ gun current, $\Phi_{\text{gun}} =$ gun flux, $\Delta =$ radial gap between the inner and outer electrodes.) If the gun current is then reduced below the threshold, the fields in the flux conserver relax toward (and decays through) a minimum energy configuration "Taylor state" with $\nabla \times \boldsymbol{B} = \lambda_{\text{fc}} \boldsymbol{B}$ where the flux conserver eigenvalue, λ_{fc}, is a function of the flux conserver geometry [9]. [For the Sustained Spheromak Physics Experiment (SSPX), $\lambda_{\text{fc}} \approx 5/R_{\text{fc}}$ where $R_{\text{fc}} =$ flux conserver radius.] Unfortunately, if the gun current pulse is extended and stays above the formation threshold, with $\lambda > \lambda_{\text{gun}}$, it necessarily produces $\lambda \gg \lambda_{\text{fc}}$ (since $R_{\text{fc}} > \Delta$) and provides free energy for driving fluctuations that degrade confinement.

In SSPX [4] (Fig. 1), a new magnetic geometry, along with careful adjustment of discharge current, allows us to produce spheromak plasmas with a wide variety of λ profiles, thereby controlling the mode behavior. While similar to many preceding gun-driven spheromaks [5], SSPX differs substantially by virtue of a set of independently programmable bias field coils. It is these coils that provide the means for flattening the λ profile during the discharge and reducing the formation threshold current by as much as a factor of 2, allowing operation with $\lambda \approx \lambda_{\text{fc}}$. By

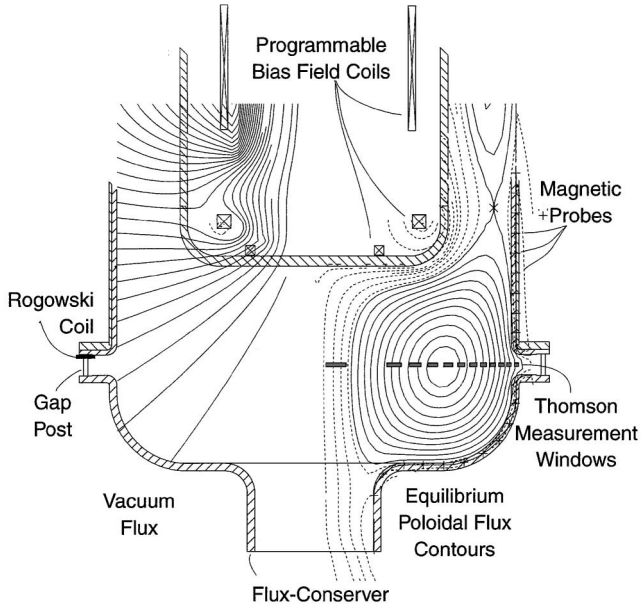

FIG. 1. SSPX cross section. Initial vacuum field configuration (left) and equilibrium (right) from CORSICA reconstruction.

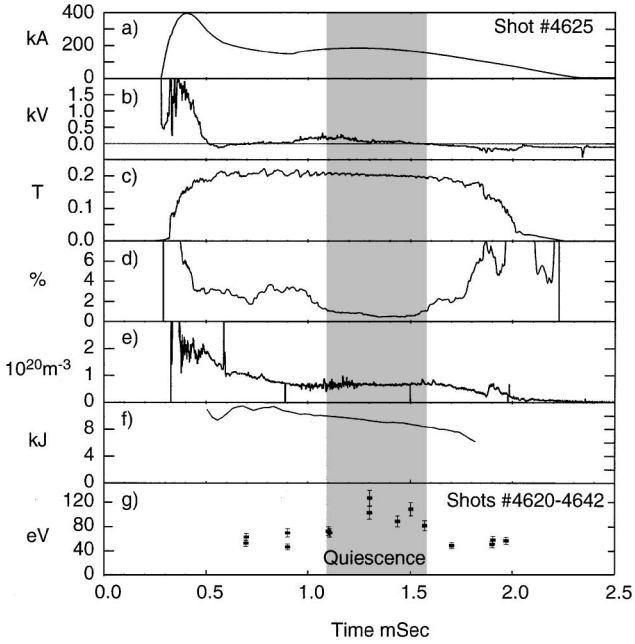

FIG. 2. Time histories for SSPX key parameters: (a) injector current, (b) injector voltage, (c) edge poloidal field, (d) rms magnetic field fluctuation level at the wall, (e) chord-averaged electron density, (f) magnetic field energy, and (g) central T_e.

carefully selecting the edge λ, it is possible to avoid driving the $n = 1$ mode to excessive amplitude while preventing decay of edge current and the onset of the $n = 2, 3, 4$ modes. The result is operation near the minimum energy "Taylor state." We note that magnetic fluctuations have also been reduced significantly in an Ohmically driven RFP by flattening λ using a technique [10] called pulsed poloidal current drive (PPCD), resulting in increases in energy confinement time (τ_E) and electron temperature (T_e).

SSPX operates with 200–500 kA injected current and ~500 V injector voltage to produce 2 ms sustained plasmas (Fig. 2) with major (minor) radius $R \sim 0.31$ m ($a \sim 0.23$ m); density, $n_{e,i} \sim 1 \times 10^{20}$ m^{-3}; toroidal current, $I_p \sim 350$ kA; edge magnetic field $B_{\text{wall}} \sim 0.25$ T and $S \sim 10^5$, with S the Lundquist number. H_2 glow-discharge cleaning, baking, He shot conditioning, and Ti gettering every 3rd shot help control impurities. A single-point Thomson Scattering (TS) system is employed to determine the T_e and n_e profiles [11]. Profiles were built up shot-by-shot in repeatable experimental conditions (<5% variation in edge poloidal field, measurement points are shown in Fig. 1). The error bars include the effects of instrument uncertainty and photon statistics. Chord-averaged n_e is also measured with a CO_2 laser interferometer aligned tangent to the magnetic axis. Ion temperature, T_i, is measured by chord-averaged ion-doppler spectroscopy (IDS) of 278.1 nm OV impurity. Magnetic field measurements are provided by an array of magnetic probes mounted flush to the inside surface of the flux conserver. Regularly spaced posts allow access for midplane diagnostics while providing a current path across the two halves of the flux conserver.

Time histories of internal profiles of $\boldsymbol{B}$, λ, $\boldsymbol{j}$, and q are inferred from a 2D ideal MHD model in the CORSICA code [4] by constructing equilibria that fit the measured edge fields and total gun current. In the code, λ is modeled by $\lambda = \lambda_{\text{edge}}(1 + \alpha\overline{\psi})/(1 + \alpha)$ where $\overline{\psi}$ is a normalized flux, varying from 0 on the magnetic axis to 1 on the separatrix, α is a fitting parameter, and $\lambda_{\text{edge}} = \lambda_{\text{gun}} = \lambda$ on the open field lines outside of the separatrix. Best fit in the quiescent regime is with $\alpha = -0.094$.

Magnetic fluctuations are calculated by Fourier mode analysis of magnetic data. There are 8 magnetic probes arrayed azimuthally in the wall just above the midplane and 14 Rogowski (current measuring) loops on the midplane gap posts. The probes and Rogowskis show very similar mode structures when analyzed, but the Rogowskis give better resolution at higher mode numbers and are used in this analysis. Figure 3 shows the time history for the $n = 1$ to 4 modes along with the profile ratio $\gamma = \lambda_{\text{edge}}/\lambda_{\text{magnetic axis}}$.

Magnetic fluctuations are reduced in amplitude during sustainment and related to changes in the λ profile. There are two current pulses in the SSPX discharge, a high current, short time-scale formation phase followed by a lower current, longer time-scale sustainment phase. All modes are present during the formation phase when the lambda profile is hollow ($\gamma > 1$). When the formation current decays, the mode amplitudes reduce as the profile relaxes ($\gamma < 1$). The discharge current then ramps back up during the sustainment phase, the λ profile is flattened ($\gamma > 0.8$), modes are suppressed, and very low mode activity is seen until the discharge current drops again. When γ drops below 0.5, large amplitude $n = 2, 3, 4$ modes are seen again. The discharge continues until the electrode voltage

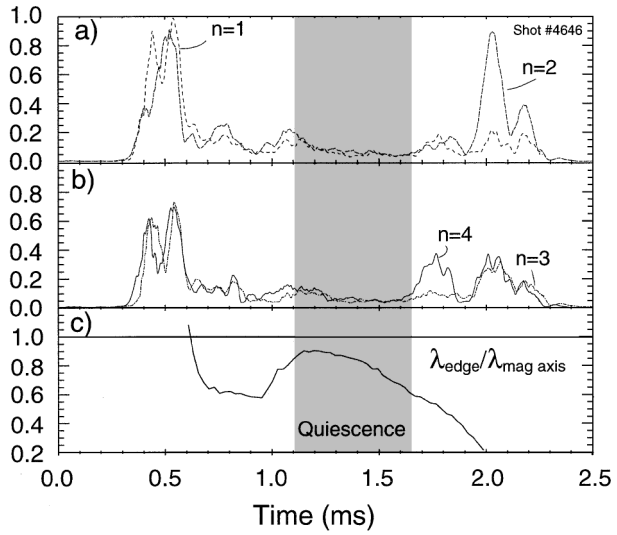

FIG. 3. MHD mode discrete Fourier analysis for No. 4646. Time evolution of (a) mode amplitude $n = 1, 2$; (b) mode amplitude $n = 3, 4$; and (c) ratio of λ_{edge} to $\lambda_{\text{magnetic axis}}$.

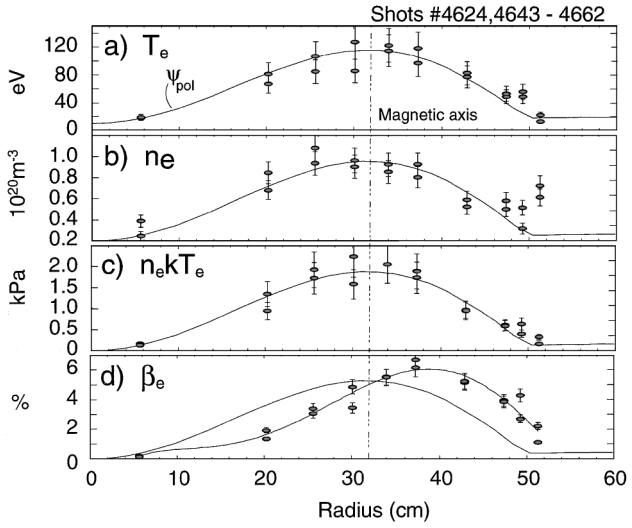

FIG. 4. Spatial profiles from Thomson scattering during quiescence. Solid lines from CORSICA-inferred poloidal flux.

reverses, a large amplitude $n = 2$ appears, and the magnetic field collapses. During low mode activity, the q profile is also rather flat ranging from 0.65 at the magnetic axis to 0.55 at $r/a = 0.9$ so there are no mode-rational surfaces with $n = 1$; and $\lambda_{\text{edge}}/\lambda_{\text{fc}} = 0.95$, i.e., close to the minimum energy "Taylor state."

Plasma temperature and magnetic field peak when the mode amplitude is small. During initial mode activity, the electron temperature T_e is 50 $\pm$ 10 eV. As the sustaining bank current peaks at 200 kA (near 1.2 ms) the mode activity drops to its lowest level, and T_e in the center of the plasma rises to its highest value of 120 $\pm$ 15 eV. Previously, T_e above 100 eV has been reported only for decaying spheromaks disconnected from the source [12,13]. The measured electron density n_e drops below 1×10^{20} m^{-3} and remains constant during this phase as does the edge magnetic field at $\sim$0.2 T. The low fluctuation period lasts for about 0.5 ms, or about a quarter of the total discharge time. After this, mode activity increases and the temperature falls to 50–60 eV.

Measured radial profiles of T_e and n_e, obtained during the quiescent period, map onto the midplane poloidal flux contours from a CORSICA fit of the magnetic probes (see Fig. 4). The T_e profile is parabolic in shape and peaks near the calculated magnetic axis. Significantly, the measurements also show that T_e, n_e, and $n_e kT_e$ lie along constant flux contours (Fig. 5) both inboard and outboard of the magnetic axis when fluctuations are low. A simple linear fit of $T_e = \text{constant}^{*}\psi_{\text{pol}}$ produces a least-squares-fit correlation coefficient of 0.95. We interpret this as supportive evidence for the existence of closed (or nearly closed) flux surfaces. We are presently unable to reconcile this with resistive MHD modeling of generic spheromaks [14] which finds open field lines.

Energy confinement time τ_E is calculated by balancing Ohmic heating P_{OH} with heat content, neglecting radiation losses (radiated power is measured to be $<$15% of input power): $dE/dt = P_{\text{OH}} - E/\tau_E$ where $E = 1.5 \int_{\text{vol}} (n_e kT_e + n_i kT_i)\, d^3r$. τ_E is determined at peak T_e where $dE/dt = 0$. P_{OH} is calculated in decaying spheromaks by observing the decay of magnetic energy in the system. This cannot be done here because the system is being driven and the magnetic energy is decaying only slightly. The input energy calculated from the discharge voltage and current cannot be used because it is difficult to quantify the electrode plasma sheath voltage drops and the energy coupled into the spheromak plasma by the dynamo. For this paper we define $P_{\text{OH}} = \int_{\text{vol}} \kappa_a \eta_{\text{sp}} j^2\, d^3r$, calculating $j(\vec{r})$ using CORSICA and making estimates of the plasma resistivity $\kappa_a \eta_{\text{sp}}$ where η_{sp} is the classical Spitzer resistivity and κ_a is an anomalous enhancement

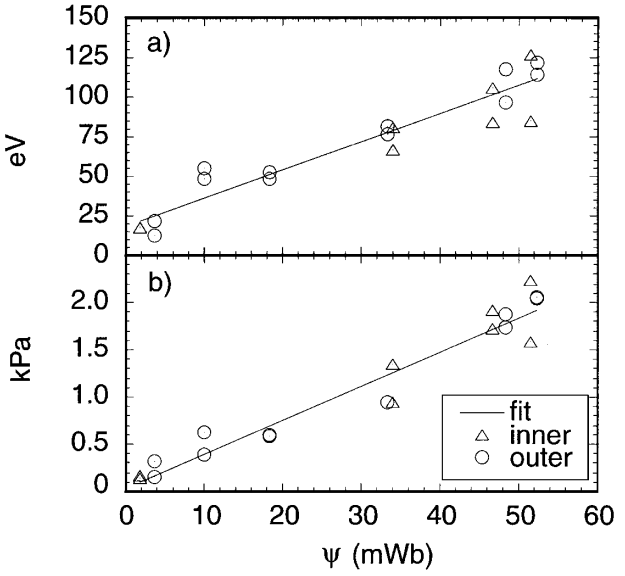

FIG. 5. Inboard and outboard T_e and $n_e kT_e$ as a function of magnetic flux.

factor. The integrals are taken over the volume within the separatrix.

Resistivity in spheromaks follows classical Spitzer scaling but with $\kappa_a = 2-4$ and most of the anomalous energy going into ion heating [15,16]. Larger fluctuations correlate with larger κ_a and produce $T_i \gg T_e$. Ion heating and κ_a are reduced for quiescent plasmas and for cohelicity magnetic reconnection [17] as takes place in spheromaks, and results in $T_i = T_e$. IDS measurements confirm this on SSPX with $T_i \gg T_e$ during formation followed by $T_i \approx T_e$ during sustainment. The ion-electron equilibration time is about twice the energy confinement time for these conditions so little energy exchange is expected. Since fluctuation amplitudes are low, we assume $\kappa_a = 2$ and include the ion contribution to the plasma energy. (This is equivalent to including only the electron thermal energy and neglecting any anomalous heating.) We use the measured T_e profile to calculate $\eta_{\rm sp}$ and estimate $Z_{\rm eff}$ two ways. Absolutely calibrated vacuum ultraviolet (VUV) spectrometer measurements and MIST impurity code calculations [18] give internal $Z_{\rm eff} = 1.5-2.0$, while edge $Z_{\rm eff}$ is estimated from the discharge resistance using the measured voltage and current, along with the T_e from TS and a determination of the current path length and cross-sectional area based on the MHD equilibrium. This yields $Z_{\rm eff} = 2.3$ in the edge region and includes anomalous effects. To be conservative, the larger edge $Z_{\rm eff}$ was used and applied to the plasma inside the separatrix.

The electron contribution to E is obtained from TS data. Error bars in T_e include the effects of instrumental uncertainties and photon statistics. The T_i measurement is chord averaged, but we assume $T_i = T_e$ and decreases with minor radius even though the majority of anomalous ion heating is expected in the edge. This results in $\tau_E \approx 150 \pm 70$ μs, the same as the highest value previously reported (CTX [19]) for a decaying spheromak and is the highest value reported for a driven spheromak.

We define the local beta as $\beta_{\rm local}(\vec{r}) = [n_e(\vec{r})kT_e(\vec{r}) + n_i(\vec{r})kT_i(\vec{r})]/[B^2(\vec{r})/2\mu_0]$ and the volume averaged local beta as $\langle\beta_{\rm local}\rangle = \int_{\rm vol}\beta_{\rm local}(\vec{r})\,d^3r/\int_{\rm vol}d^3r$. Neglecting the ion contribution, these equations give a peak local *electron* beta of $\beta_{e,{\rm local}} = 6\%$ and a volume average *electron* beta of $\langle\beta\rangle = 4\%$. Assuming $T_e = T_i$ would double this value to give a total volume average $\langle\beta\rangle = 8\%$. This is the highest value reported for a driven spheromak and comparable to the highest values reported for a decaying spheromak [20] (transient values of $\beta_{e,{\rm local}} \approx 20\%$ have been reported prior to pressure driven instability [21]).

While the edge midplane magnetic field is relatively constant while edge current is being driven, the CORSICA-calculated internal field energy within the separatrix is slowly decreasing. The gun current and voltage vary significantly during this time, so it is difficult to determine unambiguously if the configuration is being fully sustained. Modifications to extend the sustainment current pulse are being performed to explore this.

In conclusion, fluctuation levels in a driven spheromak can be substantially reduced by shaping the magnetic flux in the system with external coils, allowing operation at a predetermined ratio of current density to magnetic field. By carefully selecting the edge λ, it is possible to avoid driving the $n = 1$ mode to large amplitude and, during the decay of the plasma, also delay the onset of the $n = 2, 3, 4$ modes. During the quiescent stage, temperature profiles are a function of the axisymmetric flux found by fitting the data with an MHD equilibrium. This regime offers better confinement and higher temperatures than have been previously reported for a driven spheromak.

We gratefully acknowledge T. K. Fowler, T. R. Jarboe, N. Mattor, E. C. Morse, L. D. Pearlstein, D. D. Ryutov, and G. A. Wurden and thank the SSPX team for machine and diagnostic operation. This work was performed under the auspices of the U.S. Department of Energy by the University of California, Lawrence Livermore National Laboratory under Contract No. W7405-ENG-48.

*Permanent address: Los Alamos National Laboratory, Los Alamos, New Mexico 87545.

[1] A. H. Boozer, "Plasma Confinement," in *Encyclopedia of Physical Science and Technology* (Academic, New York, 1992), Vol. 13, p. 1.
[2] A. Rechester and M. Rosenbluth, Phys. Rev. Lett. **40**, 38 (1978).
[3] G. Fiksel *et al.,* Phys. Rev. Lett. **72**, 1028 (1994).
[4] E. B. Hooper, L. D. Pearlstein, and R. H. Bulmer, Nucl. Fusion **39**, 863 (1999).
[5] For a review of spheromaks, cf. T. R. Jarboe, Plasma Phys. Controlled Fusion **36**, 945 (1994).
[6] P. K. Browning *et al.,* Phys. Rev. Lett. **68**, 1718 (1992).
[7] A. al-Karkhy *et al.,* Phys. Rev. Lett. **70**, 1814 (1993).
[8] S. Knox *et al.,* Phys. Rev. Lett. **56**, 842 (1986).
[9] J. B. Taylor, Rev. Mod. Phys. **58**, 741 (1986).
[10] J. S. Sarff *et al.,* Phys. Rev. Lett. **72**, 3670 (1994).
[11] H. S. McLean *et al.,* Rev. Sci. Instrum. **72**, 556 (2001).
[12] T. R. Jarboe *et al.,* Phys. Fluids **27**, 13 (1984).
[13] M. Yamada, Fusion Technol. **9**, 38 (1986).
[14] C. R. Sovinec, J. M. Finn, and D. del Castillo-Negrete, Phys. Plasmas **8**, 475 (2001).
[15] J. C. Fernandez *et al.,* Nucl. Fusion **28**, 1555 (1988).
[16] T. R. Jarboe *et al.,* Phys. Fluids B **2**, 1342 (1990).
[17] S. C. Hsu *et al.,* Phys. Plasmas **8**, 1916 (2001).
[18] R. Wood *et al.,* Bull. Am. Phys. Soc. **45**, 244 (2000).
[19] F. J. Wysocki *et al.,* Phys. Rev. Lett. **65**, 40 (1990).
[20] C. W. Barnes *et al.,* Nucl. Fusion **24**, 267 (1984).
[21] F. J. Wysocki *et al.,* Phys. Rev. Lett. **61**, 2457 (1988).